Transition of a Si-As solution to the amorphous phase induced by pulsed-laser quenching

P. Baeri and R. Reitano
Dipartimento di Fisica–Università di Catania, Corso Italia 57, Catania I-95129, Italy
(Received 16 November 1988; revised manuscript received 22 February 1989)

Si-As supersaturated solid solutions obtained by ion implantation on ⟨100⟩- and ⟨111⟩-oriented Si substrates and laser annealing have been made amorphous by pulsed-laser irradiation. The transition to the amorphous phase has been detected *in situ* by time-resolved reflectivity measurements, which demonstrated that it takes place via a liquid phase as in the case of pure Si. Heat-flow computations have been employed to correlate irradiation parameters with the solidification velocity. The critical liquid-solid interface velocity to grow amorphous layers is much lower for the Si-As solution than for pure silicon. It decreases from 5 to 3 m/s with increasing As concentration from 8 to 13 at. %. Moreover, it is a factor 1.5 smaller for the ⟨111⟩ substrates than for the ⟨100⟩ ones. We explain this effect in terms of the difference between the crystalline and the amorphous melting temperature decreasing with increasing As concentration. The results are consistent with an evaluation of the free energy of Si-As solutions performed by assuming a heat of solution in the amorphous phase lower than in the crystal phase. Both experimental data and thermodynamic evaluations indicate that when the As concentration approaches an upper limit of about 15 at. % only the liquid-amorphous transition is possible since the free energy of the crystal and the amorphous phase tend to coincide.

INTRODUCTION

Fast heating ($\sim 10^{11}$ K/s) and cooling ($\sim 10^{9}$ K/s) rates achievable by pulsed-laser irradiation on thin surface layers induce transitions from stable to metastable phases and vice versa. It has been shown, for example, that the transition between liquid and solid amorphous or crystalline phases of pure silicon can be induced by nanosecond pulsed heating and there has been a considerable interest in this subject during recent years.[1,2] The phase diagram of elemental silicon is now well established and understood.

Amorphous silicon is a well-defined thermodynamic phase which undergoes a first-order solid-liquid transition at a temperature T_{al} which is 200–250 K lower than the crystal melting point T_{cl} (1685 K).[3] Its melting enthalpy (8850 cal/mol) has also been determined with good accuracy, together with its free energy with respect to the crystal phase.[4]

A necessary condition to observe the direct transition from the amorphous to the liquid phase is a fast heating rate ($> 10^{10}$ K/s) in order to avoid solid-phase crystallization.[5] The transition from liquid to amorphous silicon occurs, instead, when the solidification velocity exceeds a threshold value which depends on the substrate orientation.[6]

Indeed, dynamical observation of the solidification process using the transient conductance technique has definitely stated that the liquid-phase-epitaxial growth is suppressed in favor of the amorphous nucleation when the liquid-solid interface velocity exceeds the critical value of 15 m/s for ⟨100⟩-oriented Si substrates.[7]

In this velocity range, the liquid close to the moving interface must be substantially undercooled with respect to its equilibrium temperature with the crystal.[8] An estimate of such undercooling has been made by an analysis, based on kinetic and thermodynamic considerations, of the measured solidification velocity following 3.5-ns laser-pulse melting of silicon.[9] An almost linear relationship between undercooling and velocity with a slope of 15 K/(m/s) was derived for ⟨100⟩ silicon. Although the measurements reported in that work refer to lower interface velocities (< 6 m/s), a linear extrapolation up to 15 m/s seems very reasonable since it is based upon fitting the experimental results with a thermodynamic model of the interface response function. It also agrees, at the high-velocity limit, with a previous observation of the maximum velocity for nanosecond melts.

From the above data the liquid temperature near the interface moving at the critical velocity for the amorphization results 225 K below T_{cl}, i.e., equal to T_{al} determined by calorimetric measurements. So, within the experimental uncertainties ($\sim$ 50 K) if the liquid Si temperature is just slightly below the equilibrium temperature with the amorphous phase the solidification into amorphous Si occurs. It has been pointed out, indeed, that the liquid-to-amorphous transition, if thermodynamically allowed (i.e., if liquid temperature is below T_{al}), is preferred to the crystallization.[10]

Laser irradiation of silicon with a small amount of impurities (less than 1%) produces thicker amorphous layers than in the case of pure silicon.[11,12] This effect was explained in terms of enhancement of the amorphous nucleation probability due to impurities. It is then a merely kinetic effect since no change of the critical liquid-solid interface velocity with respect to pure Si was evidenced.

Silicon-metal liquid mixtures solidify as amorphous for much lower regrowth velocities than pure silicon does.

Pulsed-laser irradiated, codeposited metal-silicon layers were found to be amorphous when the composition was far from those of congruent compounds and closer to eutectic points in their relative phase diagram.[13] A systematic study was not attempted to see if any critical solidification velocity for amorphization exists in that case.

We note, however, that fast solidification of binary systems is an intriguing matter since phenomena related to component partitioning, leading to interface breakdown, can occur.[13]

The idea is, however, that if component partitioning is avoided, liquid undercooling will drive the nucleation of metastable phases. It has been shown that it is possible, for example, to switch the solidification between different phases of an $Fe_{50}V_{50}$ alloy by varying the liquid undercooling; a good explanation of this effect was given in terms of the relative free energies of the phases.[14] Moreover, due to competition between the nucleation of several solid phases, often a multiphase structure solidifies from the undercooled melt.[15] Our knowledge of the thermodynamic parameters of the several phases involved is inadequate to give satisfactory explanation for the appearance of these structures.

As a starting point to understand the fast solidification of a binary system, it is interesting to investigate an intermediate range of composition, i.e., the supersaturated solid solution of an element in other far from singular points, like eutectics or compounds, in the relative phase diagram. We choose silicon-dopant supersaturated solutions. The relationships between the thermodynamic parameters of the different phases of the solution (amorphous, crystalline, and liquid) will change continuously as function of the solute concentration; we will thus be able to test if the picture already established for the fast solidification of pure silicon is also valid for the solution.

The most suitable solute for this analysis is arsenic because of the very large concentration achievable in solid solution[16] and because it does not show any segregation effect in the liquid-solid interface velocity regime of our interest. It is also, among all the species which exhibit the previous characteristics, uniquely detectable by Rutherford backscattering (RBS).

EXPERIMENT

$\langle 100 \rangle$- and $\langle 111 \rangle$-oriented silicon wafers were implanted with 120-kev As^+ ions at fluences between 5×10^{16} and 10^{17} ions/cm^2. After implantation, the samples were annealed with laser pulses (30 ns, Nd laser, 1.06-μm wavelength) in order to get a crystalline Si-As solid solution. The laser energy was almost constant for each pulse (2.0 J/cm^2).

The different values of arsenic concentration in the range 7–13 at. % were obtained by one, or up to six, laser shots. Multiple pulses broaden the implanted As profile. As verified by 2-meV He RBS, the As concentration was almost constant in the uppermost (50–100)-nm-thick layer. The Si-As solid solution was crystalline throughout the entire sample as verified by channeling. All the treatments were performed at room temperature.

The thermal stability of the prepared solutions was investigated by isochronal furnace treatments of 1 h at several temperatures. Some samples were irradiated at an energy density just below the melting threshold. It was noted that the As atoms move off lattice sites at temperatures above 450 °C, while no off-lattice motion was detected in the subthreshold irradiated sample in spite of the higher temperature reached. So we conclude that the very high heating rates in the solid phase produced by pulsed-laser irradiation do not allow the As atoms to move from their initial position.

Samples prepared as above were again irradiated with the same Nd laser, with energy density ranging from 0.2 to 1.2 J/cm^2. The laser light was homogenized over a circular area of 3 mm in diameter by means of a quartz homogenizer.

A He-Ne laser beam, focused on the sample surface in the center of the pulsed-laser-irradiated area, a fast photodiode assembly, and a storage oscilloscope were used for time-resolved measurements of the surface reflectivity (TRR) in order to detect surface melting. The overall time resolution of the system was about 3 ns. The incidence angle of the He-Ne beam on the sample surface was 75°, and the polarization plane was parallel to the incidence plane. Using this geometry the reflectance difference between crystal, amorphous, and liquid silicon was enhanced with respect to the normal incidence.

2-meV He RBS in conjunction with the channeling effect technique was employed to analyze the samples after irradiation. Some samples were thinned for transmission electron microscopy.

RESULTS

Typical transient reflectance curves are reported in Fig. 1. These reflectivity signals refer to $\langle 100 \rangle$-oriented samples with 11-at. % As concentration (the same sample to which Fig. 4 refers), irradiated with different energy-density pulses. The signals obtained for irradiations between 0.2 and 0.3 J/cm^2 are shown as dashed lines. The intensity of the reflected He-Ne laser beam does not reach the value corresponding to the liquid reflectivity but progressively increases with increasing energy density of the laser pulse between 0.2 and 0.3 J/cm^2.

Such a behavior was previously observed for both pure Si and Ge (Ref. 17) and is not to be ascribed to a poor time resolution of the measurement; instead, it is in part due to the formation of a liquid layer thinner than the probe light-absorption length ($\sim$10 nm), and to some microinhomogeneity of the laser-pulse intensity not completely avoided by the quartz rod. We believe the latter to be the main reason of this near-threshold behavior. The surface melting threshold, E_{th}, was assumed to be the energy density at which the midpoint value between the solid and the liquid reflectivity is reached by the signal of the reflected He-Ne laser beam. For this particular sample it is $E_{th}=0.25$ J/cm^2.

The solid lines refer to higher-energy-density irradiations of 0.45 and 0.8 J/cm^2. The surface melt is well evidenced in these cases by the plateau of the signal at the liquid reflectivity value. The reflectivity drops again to

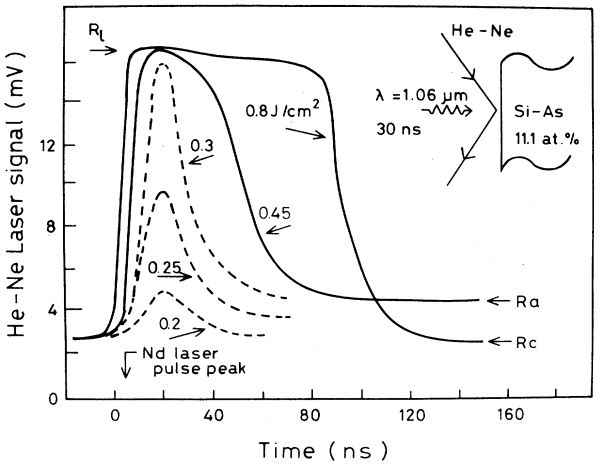

FIG. 1. TRR signals for ⟨100⟩-oriented Si with 11.1 at. % As irradiated with 30-ns Nd-laser pulses. Dashed lines: near-melting-threshold energy-density irradiations. Solid lines: energy-density irradiations above the melting threshold. Arrows marked R_c, R_a, and R_l indicate the signal level for crystal, amorphous, and liquid Si, respectively.

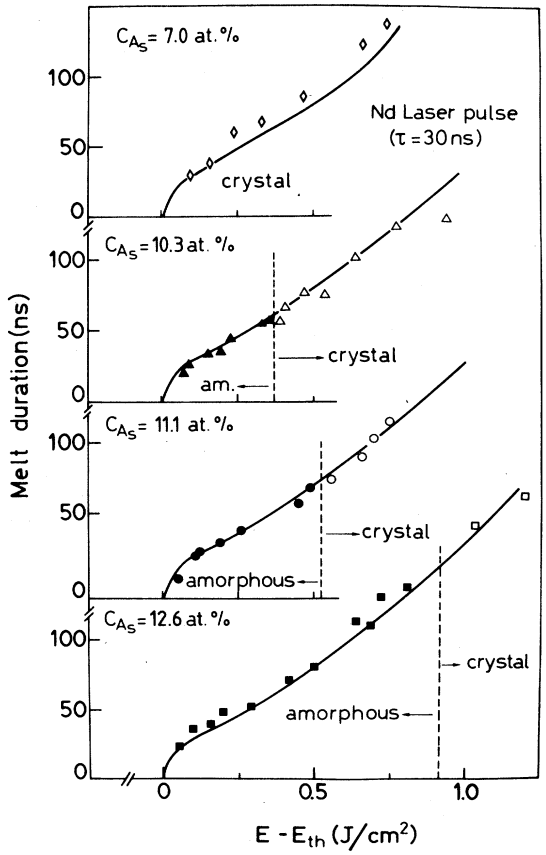

FIG. 2. Melt duration vs energy density above the melting threshold of 30-ns Nd laser pulses for several As concentrations of ⟨100⟩-oriented Si. Open and solid symbols indicate the liquid-crystal or liquid-amorphous transitions, respectively. Solid lines are the calculated melt durations.

the value of the solid phase after 45 and 90 ns for the 0.45- and 0.8-J/cm^2 irradiation, respectively. However, the final levels are different. At the lower-energy-density irradiation it corresponds to the amorphous reflectivity, indicating that the liquid-to-amorphous transition took place. For the higher-energy-density irradiation, instead, the final level is the same as the starting one, indicating that the crystal-liquid-crystal transition was induced by the laser pulse.

Transient reflectivity measurements were performed for several irradiation energy densities E and for different As concentration C_{As}. We found that the surface-melting-threshold energy density E_{th} increasing with decreasing C_{As}. We measured a minimum value of 0.25 J/cm^2 for the samples with the highest As concentrations (12.6 and 11.1 at. %), while for the lower one (7 at. %) we measured E_{th}=0.4 J/cm^2. This behavior is due to the dependence of both the melting temperature and the Nd light-absorption coefficient on the As concentration of our samples.

In the following, we will present all our results as function of the parameter $E-E_{th}$, which is more appropriate than E for a description of the melting and solidification dynamics, as we will show in the following section.

In spite of the different melting thresholds, the trend of the surface-melt duration versus the energy-density difference ($E-E_{th}$) is the same for all the Si-As solutions as shown in Fig. 2. The data refer to ⟨100⟩-oriented samples with 7-, 10.3-, 11.1-, and 12.6-at. % As concentrations, respectively.

The experimental points for the different samples all lie on the same solid line, which is plotted four times in the picture. This line is the result of heat-flow calculations which will be illustrated in the next section. Open and solid symbols indicate irradiations which induced the crystal-liquid-crystal or the crystal-liquid-amorphous transitions, respectively. The energy-density value (indicated by a dashed line in the graph) below which the samples solidified as amorphous increases with increasing arsenic concentration. The samples with the lowest As concentration (7 at. %) remained single crystalline for all the employed energy-density irradiations.

Similar results have been found for the ⟨111⟩-oriented samples. In Fig. 3 the melt durations as functions of $E-E_{th}$ are reported for 8.7- and 10-at. % arsenic concentration. The trend of the data is similar to that of the ⟨100⟩-oriented samples, but the energy-density thresholds to obtain complete recrystallization are remarkably higher. In particular, for ⟨111⟩-oriented silicon with 10.0-at. % As concentration for liquid-to-amorphous transition occurred for $E-E_{th}$ values below 0.85 J/cm^2, while in the ⟨100⟩ samples with the same dopant concentration, amorphous formation was found only for $E-E_{th}$ below 0.35 J/cm^2.

The results obtained by TRR measurements were confirmed by the RBS analysis of the irradiated samples. In Fig. 4 the RBS spectra of the as-prepared sample with a concentration of 11.1 at. % As and after further irradia-

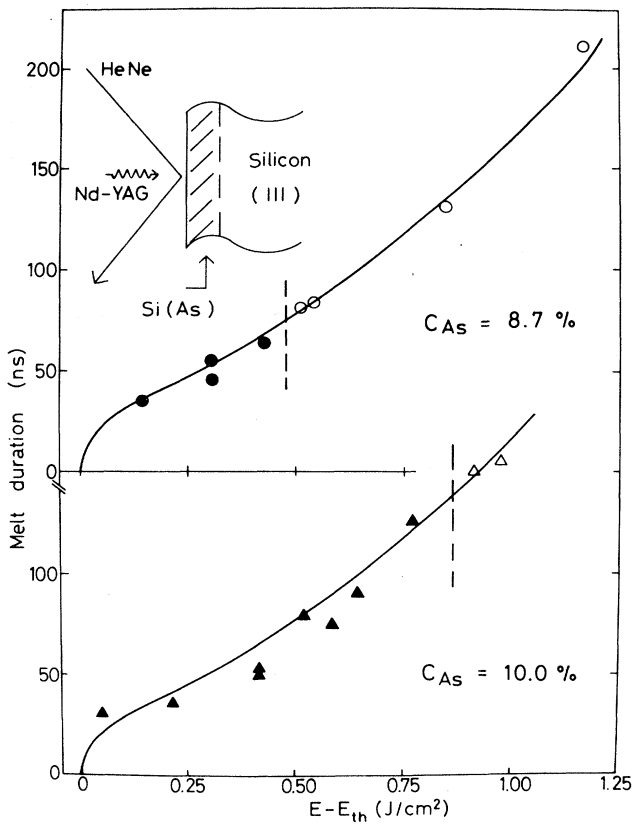

FIG. 3. Same as Fig. 2, but for ⟨111⟩-oriented samples.

tion with 0.45 J/cm^2 are reported. The solid line represents the random spectra of both samples; the irradiation with 0.45 J/cm^2 energy density, in fact, did not produce any further appreciable diffusion of As atoms compared with the diffusion induced by the adopted annealing procedure (three shots at 2 J/cm^2 energy density for this sample). The 100-keV plateau extent in the As signal corresponds, in our glancing detection geometry, to a 75-nm-thick layer with 12.5-at. % As concentration.

The channeling spectrum is reported for the starting sample as solid dots. The minimum yield in the silicon signal is about 4%, indicating a good crystal quality. The minimum yield in the arsenic signal is 13%, indicating that the substitutional concentration is 11.1 at. %. In all the samples, the substitutional concentration was slightly lower than the total concentration. All throughout the paper we will refer to the former.

The aligned spectrum for the 0.45-J/cm^2-irradiated sample is shown as open circles. An amorphous layer 50-nm thick is evident from both the Si and As signals. The presence of the amorphous phase was checked by electron-diffraction analysis.

The thicknesses of the amorphous layers are reported in Fig. 5 as a function of $E - E_{th}$ in the ⟨100⟩-oriented samples for several As concentrations. The two solid lines delimiting the shadowed region are the results of computations of the maximum melt-front penetration,

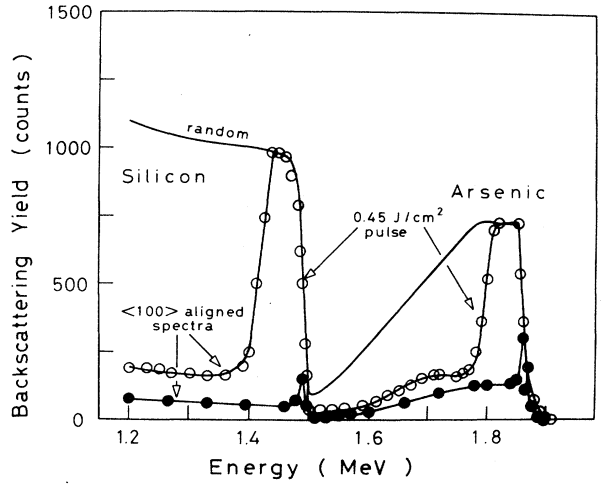

FIG. 4. 2-MeV-He RBS spectra of a crystalline Si-As alloy obtained by As implantation and laser annealing. Solid line, random spectrum; solid dots, channeling along the ⟨100⟩ direction; open dots, channeling along the ⟨100⟩ direction after further irradiation with 30-ns Nd-laser pulse at 0.45 J/cm^2.

which will be detailed in the next section.

Just above the melting threshold, the thickness of the amorphous layers increases with increasing energy density, following the thickness of the molten layer very closely. Maximum thicknesses are obtained for well-defined energy densities of 0.25, 0.3, and 0.4 J/cm^2 above E_{th} for the 10.3-, 11.1-, and 12.6-at. % As concentration, respectively.

After further increase of the irradiation energy density, the melt depth increases almost linearly, but the

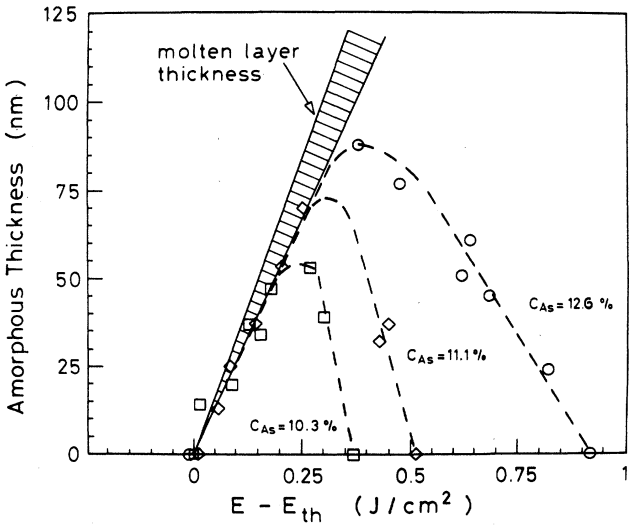

FIG. 5. Open symbols: measured thickness of the amorphous layers produced by 30-ns Nd-laser-pulse irradiation on Si-As solid solution for several As concentration C_{As}. Dashed lines: fit of experimental data. Solid lines: calculated melt depth. The abscissa sacle is the energy density of the laser pulse measured above the surface melting threshold.

amorphous-layer thickness decreases and the amorphous layer vanishes at energy-density values which coincide with the thresholds for full recrystallization as derived by the TRR measurements.

It is evident that in the low-energy-density regime, the amorphous Si-As solution is formed almost immediately at the solidifying interface, as observed in lightly doped Si.[11] At high energy densities, instead, the epitaxial growth of the crystal proceeds for a considerable thickness before the amorphous phase nucleates and exhibits a behavior similar to that of pure silicon.[5,6] However, the thicknesses of the amorphous layers produced in our experiments are at least a factor of 3 higher than those obtained in the pure-Si case.

HEAT-FLOW CALCULATIONS

The temperature, as well as the melt-front evolution of the irradiated samples, can be calculated following a widely used heat-flow computational approach.[18] As we deal with samples having different As content, it is, in principle, expected that the result of such calculations will be different for the various samples.

The optical and thermal parameters needed as input data are reported for pure Si in Table I. We adopted these values for the pure-Si inner layers, while for the Si-As solution layer, they must be reevaluated as functions of the As concentration so that they become depth dependent.

In particular, the major differences with the pure-silicon case arise from the great influence of the As concentration on the absorption coefficient at the Nd-laser wavelength and on the melting temperature of the Si-As solution. We shall discuss briefly the relevance of these two topics.

The absorption coefficient of the Si-As solid solution in the 10-at. % As concentration range is of the order of 10^5 cm^{-1},[19] well above that of pure silicon (see Table I). As a consequence, most of the laser-pulse energy is absorbed into the Si-As layer, while the remaining part is very diluted in the substrate, where it produces negligible heating. Different values of the absorption coefficient [in the (10^4-10^5)-cm^{-1} range] due to the different As content will result in different melting-threshold energy densities. We perform calculations and obtained E_{th} values ranging from 0.32 to 0.5 J/cm^2 for absorption coefficients ranging from 5×10^5 to 5×10^4 cm^{-1}, respectively.

However, thermal diffusion into the bulk spreads out the temperature profile over a larger depth than the outer 200-nm Si-As layer where the laser light is absorbed. In fact, since the heat-diffusion coefficient is of the order of 0.1–1 cm^2/s, just during the 30-ns heating time the heat-diffusion length is about 1 μm and it becomes even larger during solidification. The temperature gradient is then independent of the actual value of the light-absorption coefficient in that layer. It is the same for the same amount of energy density above the melting threshold $E-E_{th}$. Calculations performed using absorption coefficients in the range specified above gave an average temperature gradient of 9×10^6 K/cm over the outermost 0.5 μm at the respective melting thresholds.

Since the melt-front dynamics is essentially determined by the temperature gradient,[18] the computed melt-front evolution is the same for samples with different As concentrations for the same fixed value of $E-E_{th}$.

Let us now discuss the influence of the thermal parameters on the heat-flow computations.

The different melting temperatures of our samples will change the melting-threshold energy density; in contrast, the melt-front dynamics does not change since it does not produce any effect on the temperature gradients.

However, our samples exhibit a depth-dependent melting temperature due to the As concentration gradient and this does affect the melt-front velocity.

In fact, during solidification the heat flux through the liquid-solid interface has to balance the released latent heat, but it must also depress the liquid temperature more and more to allow the solidification of the outer layers that have lower solidification temperatures. This produces a slowing down of the interface upon going toward regions with greater As content, as has been observed experimentally.[20]

Similar effects are produced during melting since the liquid-solid interface temperature must increase to allow melting of the inner layers with lower As content. So the maximum melt depth will depend on the As depth profile and it is smaller the greater the As concentration gradient.

In our calculations we adopted the melting temperature T_m and the melting enthalpy ΔH_m of the crystalline Si-As solution shown in Fig. 6 as function of the As concentration. The derivation of these curves will be explained in the next section.

The calculated melting-threshold energy density for our samples ranges from 0.25 to 0.5 J/cm^2 on going from 13- to 7-at. % As concentration and assuming a light-absorption coefficient ranging from 2×10^5 to 5×10^4 cm^{-1} for the same As concentration range.

At energy densities above E_{th} the computed maximum melt depth increases almost linearly with $E-E_{th}$, as shown in Fig. 5 together with the experimentally determined amorphous layer thicknesses. The spread of our results using the different melting-temperature–depth relationship to account for the different As-concentration profiles is shown by the dashed area; the two solid lines were computed for samples with the highest (12.6 at. %) and lowest (7 at. %) As concentrations, which also correspond to the highest and lowest concentration gradients, respectively.

The time during which the surface remains liquid is

TABLE I. Optical and thermal parameters of pure silicon used in the heat-flow calculations.

Absorption coefficient (cm^{-1})	$5e^{-T(K)/430}$
Reflectivity	0.32
Specific heat (cal/mol K)	$5.45+(0.92\times10^{-3})T-(0.85\times10^5)T^{-2}$
Thermal conductivity (W/cm K)	$1585T^{-1.229}$
Melting temperature (K)	1685
Melting enthalpy (cal/mol)	12 000

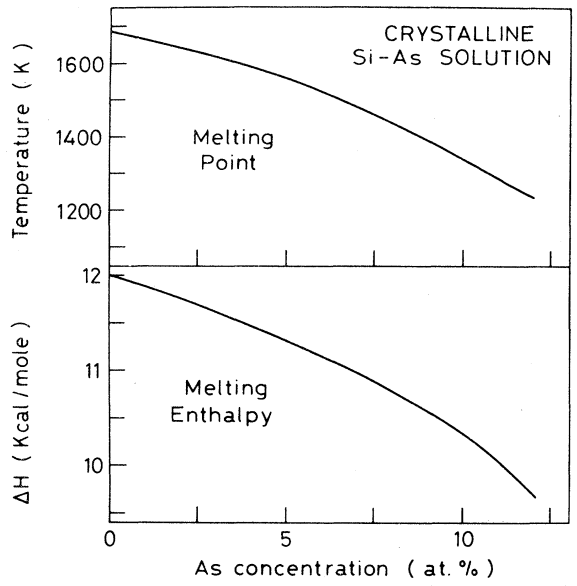

FIG. 6. Computed melting temperature (upper) and melting enthalpy (lower) of a crystalline Si-As solution as a function of the arsenic concentration.

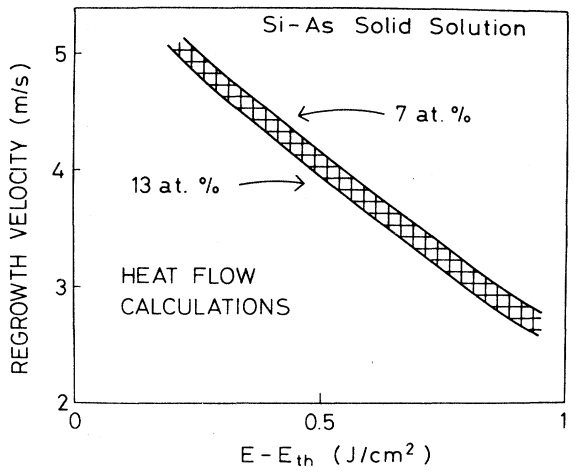

FIG. 7. Calculated solidification velocity as a function of the energy density above the melting threshold, for a 30-ns Nd-laser pulse on Si-As solid solutions. The spreading of the calculated values for different As-concentration profiles is within the dashed area.

unaffected by the depth-dependent melting temperature since the maximum melt-depth reduction is balanced by the reduced velocity during solidification. In fact, the measured values of the melt duration reported in Figs. 2 and 3, although they refer to samples with different As contents and depth profiles, all lie on the same curve, which agrees very well with the calculated one.

The good agreement of both the computed molten layer thickness and surface melt duration with the experimental data gives us confidence in our computation approach and thus in the computed liquid-solid interface velocity values for which no direct measurement is available. They are reported in Fig. 7 as functions of the energy density.

These velocities refer to the outermost layer with constant As concentration, which is the region of interest for our purposes since all the amorphous-crystal interfaces of the laser-amorphized samples were found within this layer. The velocity varies from 5 m/s for irradiation energy density near the melting threshold to 2.5 m/s for $E-E_{\rm th}=1.0$ J/cm^2. The cross-hatched area represents the dispersion of the calculation results arising from the different As depth profiles of our set of samples; the lower and upper curves refer to the samples with the higher and lower As concentration.

We conclude this section by discussing the critical velocity values to solidify pure amorphous silicon from the melt.

The first estimates, made by the one of the present authors, of the critical velocity for the liquid-to-amorphous transition in pure silicon were done by heat-flow computations related to 2.5-ns pulsed uv-laser irradiations of pure Si. They were 18 and 12 m/s for ⟨100⟩- and ⟨111⟩-oriented substrates, respectively.[6] In that paper, however, the maximum velocity (which occurs near the maximum melt-front penetration) and not the one at the depth where the amorphous phase was effectively formed was reported. We recalculated the latter obtaining values of 15 and 10 m/s for the ⟨100⟩ and ⟨111⟩ orientations, respectively. The calculated value for ⟨100⟩-oriented silicon agrees very well with the measured value using the transient conductance technique,[7] thus giving confidence in the one computed for the ⟨111⟩ case.

DISCUSSION AND THERMODYNAMIC EVALUATIONS

The results of heat-flow calculations allow us to correlate the measured energy densities of the laser pulse to induce the liquid-to-amorphous transition with the regrowth velocity. Moreover, knowing the As concentration for each sample, it is possible to correlate this last quantity with the critical solidification velocity. The results are plotted in Fig. 8(a) both for the ⟨111⟩ (circles) and ⟨100⟩ (squares) orientations. The experimental points of pure Si are also reported. For the same As concentration, the critical amorphization velocity is lower for the ⟨111⟩ substrates than for the ⟨100⟩ ones as for pure silicon.

The velocity-undercooling relationships can be used to convert the abscissa scale of Fig. 8(a) into a temperature scale. The undercooling for liquid-epitaxial regrowth along the ⟨100⟩ direction in Si is 15 K/(m/s) (Ref. 9) and molecular-dynamics computations[21,22] allow us to extend this result to the ⟨111⟩ direction of growth by scaling with a factor of 1.5. We thus assumed 22.5-K/(m/s) undercooling for the liquid-phase epitaxy along the ⟨111⟩ direction. The liquid temperatures associated with the two different critical velocities for the ⟨111⟩- and ⟨100⟩-oriented pure-Si samples are then the same.

By replotting the ⟨100⟩ and ⟨111⟩ data of Fig. 8(a) in

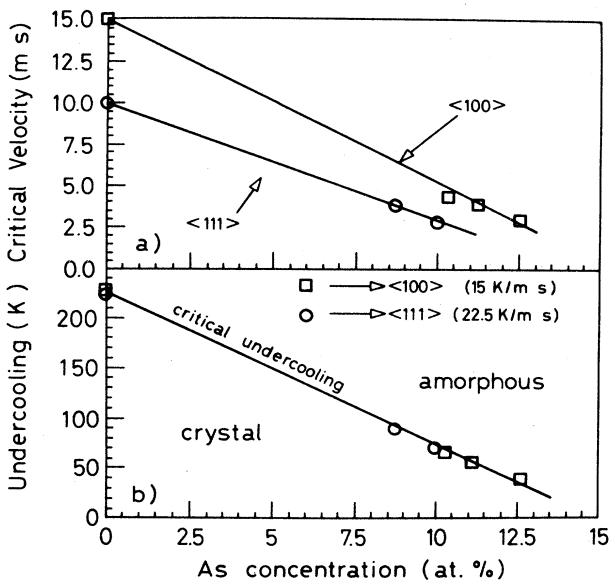

FIG. 8. (a) Critical solidification velocity to suppress the epitaxy in favor of the amorphous nucleation for a Si-As solution as a function of the As concentration. Lower curve: ⟨100⟩ epitaxy. Upper curve: ⟨100⟩ epitaxy. (b) Critical undercooling of the Si-As liquid solution, with respect to its equilibrium temperature with the crystal phase, to nucleate the amorphous as a function of the As concentration.

terms of the amount of undercooling through its relationship with the velocity, a single curve has been obtained as shown in Fig. 8(b).

The solid line labeled "critical undercooling" separates two regions: in the upper region solidification will result in an amorphous layer, while in the lower region full epitaxial regrowth will take place. It is also possible to extrapolate toward a critical value of As concentration (about 15 at. %) at which no undercooling of the liquid below its equilibrium temperature with the crystalline solid is needed to solidify the amorphous phase.

To understand this behavior of the critical undercooling we will evaluate the free energies of the Si-As solution.

Using the available thermodynamic data,[23,24] we are able to compute the free energy of the liquid and crystal phases of pure Si and As, respectively.

For the Si-As liquid solution we can use the regular-solution model valid in the range (0–40)-at. % As concentration.[25]

In the solid phase, no experimental data are reported in the concentration range of interest. So we extrapolated the available data about the activity coefficients of the Si-As solid solution to our concentration range. The activity coefficient of As has been measured at high temperature in the (0–3.5)-at. % As concentration range.[26] We can extrapolate these data at higher As concentrations since they show a very weak dependence on both temperature and As concentration on increasing the latter. For the activity coefficient of Si, a general expression as a function of temperature and As concentration was proposed.[27]

We were then able to compute the free energy of the solid crystalline phase G^c, and of the liquid phase G^l, as a function of As concentration and temperature. From these data we computed the melting point of the crystalline solution, i.e., the temperature T_m at which $G^c=G^l$. The calculated values of T_m are reported in Fig. 6(a) as function of the As concentration.

The melting point strongly decreases with increasing C_{As} and it reaches 1480 K for $C_{As}=7$ at. % and 1200 K for $C_{As}=13$ at. %. In particular, we note that our calculated melting-temperature reduction of 200 K for $C_{As}=7$ at. % agrees satisfactorily well with the estimate of 150 K at the same As concentration reported in Ref. 20.

In order to compute the melting enthalpy, we used the linear approximation $G^l-G^c=\Delta H_m-T\Delta S_m$, where ΔH_m and ΔS_m are the enthalpy and entropy of the liquid-solid transition, respectively, and $T_m=\Delta H_m/\Delta S_m$. We derived ΔS_m from the slope of the (G^l-G^s)-versus-T curves and thus evaluated ΔH_m, which is reported in Fig. 6(b).

By comparing Figs. 6(a) and 6(b), we note that the computed reduction of the melting point below that of pure Si is almost proportional to the reduction of the melting enthalpy, while ΔS_m changes very little with C_{As}. The reduction of ΔH_m arises from a large positive term of the heat of solution, ΔH^c_{sol}, in the crystal phase together with a relatively small negative heat of solution in the liquid phase, ΔH^l_{sol}. As an example we report in Table II the computed values of ΔH_m, ΔS_m, ΔH^c_{sol}, and ΔH^l_{sol} for $C_{As}=10$ at. %.

The heat of solution can be regarded as the sum of three terms:[28] a structural term ΔH_{struct}, which accounts for the variation of the lattice stability, an elastic term ΔH_{elast}, which is the elastic energy due to the atom-size mismatch, and a chemical term ΔH_{chem}, which is related to the chemical bond of the Si-As pairs. The last term has the same value in all the phases; the structural and elastic terms are obviously not present in the liquid phase so that $\Delta H^l_{sol}=\Delta H_{chem}$.

With a reasonable assumption we can evaluate these three terms as functions of the As concentration. As an example, they are reported in Table II for $C_{As}=10$ at. %.

Now let us discuss the case of the amorphous solid solution. We adopted the free energy of the covalently bonded amorphous phase[4] for pure Si, while for pure amorphous As a frozen-liquid, glassy phase was assumed.

In the heat of solution in amorphous phase, ΔH^a_{sol}, one obviously neglects the structural term and if one treats, following Ref. 28, the amorphous phase as a simple liquidlike model as in the metallic systems, it is $\Delta H^a_{sol}=\Delta H^l_{sol}=\Delta H_{chem}$. However, in our case we deal with a covalent material since amorphous silicon is a fourfold-coordinated system rather than an eightfold- or tenfold-coordinated system like liquid Si and, as a more realistic approximation, we suggest

$$\Delta H^a_{sol}=\Delta H_{chem}+\beta\Delta H_{elast} \quad \text{with } \beta<1 ,$$

since some local elastic energy, although reduced by the

TABLE II. Computed melting enthalpy, entropy and temperature, and heats of solution for Si-As solutions with 10-at. % As concentration. For comparison, values for pure silicon are also reported.

	Pure silicon		$Si_{0.9}As_{0.1}$		
	Crystal	Amorphous	Crystal	Amorphous	Liquid
ΔH_m (cal/mol)	12 000	8860	10 317	7368	
ΔS_m (cal/mol K)	7.122	6.07	7.68	6.07	
T_m (K)	1685	1460	1343	1214	
ΔH_{sol} (cal/mol)			815	255 ($\beta=1$)	−315
ΔH_{struct} (cal/mol)			560	0	0
ΔH_{chem} (cal/mol)			−315	−315	−315
ΔH_{elast} (cal/mol)			570	570 ($\beta=1$)	0

factor β with respect to that of the crystalline phase, should be included. Amorphous Si does have a bond disorder that does not exist in the crystalline phase. Thus the local strain energy due to the As atoms is much better accommodated in the amorphous phase than it is in the crystalline phase. For this reason we believe the factor β to be less than unity, but not equal to zero as it should be for a glassy metallic phase.

Even in the approximation of $\beta=1$, ΔH^a_{sol} is lower than the enthalpy of solution in the crystal phase, as shown in Table II for $C_{As}=10$ at. %.

Moreover, we will neglect the dependence of the amorphous melting entropy on the As concentration as we found in the crystalline phase. We are then able to evaluate the free energy of the amorphous solid solution and to compute its melting point as we did for the crystalline solution.

As an example of these calculations, the free-energy diagrams are reported in Fig. 9, taking as a reference the free energy of the crystalline phase. This example refers to $C_{As}=10$ at. % and assumes $\beta=1$. For comparison, the case of pure silicon is reported on the right-hand-side of the same figure.

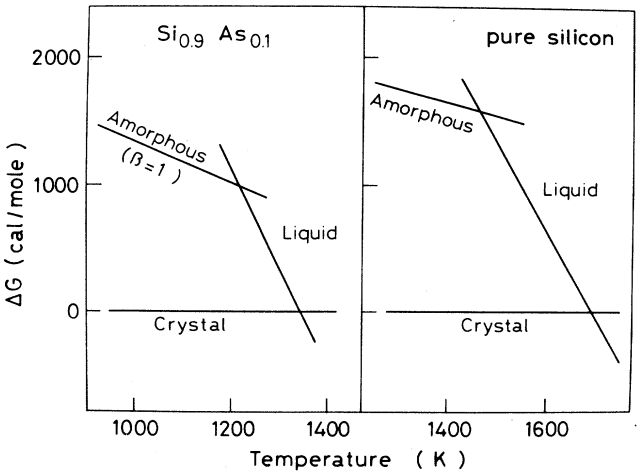

FIG. 9. Free energy of a $Si_{0.9}As_{0.1}$ solution (left) and of pure Si (right) for the amorphous and liquid phase taking as a reference the crystal phase.

It is evident that the difference between the crystal and amorphous free energy in the solution is lower than it is in pure Si. This is, in fact, the main effect of the assumption of a reduced heat of solution in the amorphous phase with respect to the crystalline phase.

The equilibrium temperatures of both solid phases combined with the liquid one are lower in the solution than in pure Si, but their difference is smaller.

The melting point of the amorphous is reported in Fig. 10(a) for $\beta=1$ as a function of the As concentration; the melting point of the crystalline solution is also reported for comparison in the same figure (dashed line). The melting point of the amorphous solution decreases with increasing C_{As} in a less pronounced way than that of the crystal solution.

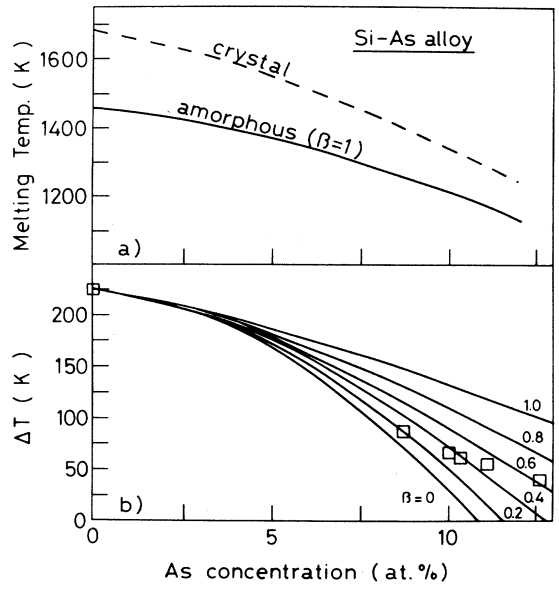

FIG. 10. (a) Computed melting temperature of crystalline (dashed line) and amorphous (solid line) Si-As solid solutions as a function of As concentration. (b) Computed difference between the crystal and amorphous melting points for different values of the parameter β (see text); the squares are the measured critical undercooling to obtain the liquid-to-amorphous transition [same data of Fig. 8(b)].

For $C_{As}=0$ the difference between the crystalline and amorphous melting point is 225 K, i.e., the same as for pure Si; with increasing As concentration the difference becomes smaller and smaller until it vanishes for $C_{As}=20$ at. % (for $\beta=1$).

In Fig. 10(b) we report the difference between the crystalline and amorphous melting points as a function of the As concentration for several values of the parameter β. The lowest curve has been computed by evaluating the enthalpy of solution in the amorphous phase as due only to the chemical contribution ($\beta=0$), while the upper curve includes an elastic term equal to that of the crystalline phase ($\beta=1$).

The experimental points reported in the same picture are the critical undercooling to nucleate the amorphous phase as derived from our experiments [see Fig. 8(b)]. From comparison of the calculated curves and the experimental data, it is possible to conclude that a concentration-dependent value of β, ranging from 0.2 to 0.6, should be assumed to obtain a satisfactory agreement between them.

It must be pointed out that this estimate of β may be incorrect since it is based on the assumptions and approximations used for the thermodynamic description of the crystalline and amorphous solutions. However, the evaluation of the elastic term in the heat of solution for the amorphous phase is outside the scope of this work. The results in Fig. 10 instead demonstrate clearly that the lower heat of solution in the amorphous phase with respect of the crystalline phase accounts for the observed dependence of the critical undercooling for amorphization on the As concentration.

SUMMARY AND CONCLUSIONS

The experimental results demonstrate that the pulsed-laser-induced amorphization of a supersaturated crystalline Si-As solution in the (7–13)-at. % As concentration range exhibits the same qualitative features as pure silicon. The transition to the amorphous phase takes place via the liquid phase when the solidification velocity exceeds a critical value which depends on the substrate orientation.

However, a quantitative difference between the two cases is evident both in the critical velocity values and in the thickness of the amorphous layers produced.

In fact, it is possible to induce amorphization employing a laser which, for its pulse duration and wavelength, it is not feasible to induce solidification velocities high enough to amorphize pure silicon. We obtained amorphous layers on ⟨100⟩-oriented substrates in the (3–5)-m/s solidification velocity range, while pure Si solidifies as amorphous only at velocities greater than 15 m/s. Moreover, the thickness of the amorphous layers is considerably greater for the Si-As solution than for pure Si.

A strong correlation between the As concentration and the critical velocity has also been found. All our data are consistent with the hypothesis that the difference between the crystal and amorphous melting points decreases with increasing As concentration. This temperature difference is, in turn, the minimum amount of undercooling with respect to the crystal-liquid equilibrium temperature needed to nucleate the amorphous phase from the liquid. At the moving solid-liquid interface the undercooling is driven by the solidification velocity; thus the critical velocity will decrease with increasing As concentration. By thermodynamically modeling the Si-As solution, we have shown that the heat of solution in the crystal phase is important and considerably depresses the melting enthalpy and the melting point with respect to pure silicon. Since the heat of solution in the amorphous phase must be lower than in the crystalline phase, the reduction of the melting point as a function of the As concentration is less pronounced for the amorphous than for the crystalline phase.

In order to make this explanation plausible, a series of assumptions has been made all through the text which is now summarized for the sake of clarity.

First, it was assumed that the liquid undercooling at the critical velocity for amorphous-phase nucleation is nearly equal to the difference between the crystal and amorphous melting points. This assumption was justified when we discussed Refs. 9 and 10.

The second assumption is that the velocity response functions for the Si-As solution and pure Si are the same. These are the more critical assumptions for our explanation. If one or both are not true, kinetical aspects of the amorphization process will become more relevant than the pure thermodynamical analysis given here. The thermodynamic analysis is based on a crude extrapolation to our As concentration of the thermodynamic parameters measured in a different concentration range. This assumption is not so crucial as the first two. The exact evaluation of the T_0 curve of the Si-As system is unessential since it is the difference between the crystal and amorphous melting points that allows the amorphization at lower velocity and not their absolute values. The substantial agreement between the only available datum on the Si-As solution melting point[20] and the result of our calculations is sufficient for the purposes of this work.

Finally, we have modeled the amorphous Si-As solution as a phase with thermodynamical properties in between those of the crystalline and a glassy phase by assuming its heat of solution to be a nonzero fraction of that of the corresponding crystalline solution. If the first two assumptions are valid, the latter is demonstrated by our experimental data, while a better modeling of the crystalline solution (if more precise thermodynamic parameters should become available) will only affect the best-fit value of the parameter β.

The picture presented is self-consistent and strongly indicates that at high As concentrations ($>15\%$) the amorphous phase becomes more stable than the crystalline one at the solidification temperature. At these concentrations, provided that the quenching rate is high enough to prevent dissociation of different phases (such as, i.e., As precipitates), the amorphous phase should solidify at any liquid-solid interface velocity.

Moreover, we note that the simple rule given for many metal-silicon systems, for which the amorphous phase can be laser quenched only at concentrations close to eu-

tectic points, does not apply in the Si-As system; in this case, in fact, the eutectic point is at about 40-at. % concentration, very far from the investigated concentration range. The reason is probably related to the low As diffusivity compared with that of the transition metals, which prevents long-range motion. In this latter case, in fact, segregation effects, resulting mainly in cellular structures, have been evidenced.

Finally, we may give the following thermodynamic criterion to determine the upper limit of solute concentration in a supersaturated substitutional solid solution obtainable by fast solidification: it is the concentration at which the melting curve (i.e., the so-called T_0 curve) of the crystalline solution reaches the value of the melting point of the amorphous solution [see Fig. 10(a)]. Above this concentration and at this temperature the amorphous phase is a more stable phase than the crystalline one. This criterion is more restrictive than the one proposed by Cahn,[29] which indicates as limiting concentration the one at which the T_0 curve reaches 0 K. In this case, in fact, the supersaturated solid solution should be unstable with respect to the liquid solution at every temperature.

ACKNOWLEDGMENTS

Thanks are due to Professor G. Foti and Professor E. Rimini for many helpful discussions, and to Mr. N. Marino for his assistance in the neodymium-laser operations. This work was supported by "Progetto finalizzato materiali e dispositivi per l'elettronica a stato solido."

[1]See, for example, as a review paper, P. S. Peercy, M. O. Thompson, and J. Y. Tsao, in *Beam Solid Interaction and Transient Processes,* Vol. 74 of *Materials Research Society Symposium Proceedings,* edited by M. O. Thompson, S. T. Picraux, and J. S. Williams (MRS, Pittsburgh, 1987), p. 15.

[2]J. M. Poate, Nucl. Instrum. Methods **209-210**, 211 (1983).

[3]M. O. Thompson, G. J. Galvin, J. W. Mayer, P. S. Peercy, J. M. Poate, D. C. Jacobson, A. G. Cullis, and N. G. Chew, Phys. Rev. Lett. **52**, 2360 (1984).

[4]E. P. Donovan, F. Spaepen, D. Turnbull, J. M. Poate, and D. C. Jacobson, J. Appl. Phys. **57**, 1795 (1985).

[5]P. Baeri, G. Foti, J. M. Poate, and A. G. Cullis, Phys. Rev. Lett. **45**, 2036 (1980).

[6]A. G. Cullis, H. C. Webber, N. G. Chew, J. M. Poate, and P. Baeri, Phys. Rev. Lett. **49**, 219 (1982).

[7]M. O. Thompson, J. W. Mayer, A. G. Cullis, H. C. Webber, N. G. Chew, and J. M. Poate, Phys. Rev. Lett. **50**, 896 (1983).

[8]D. Turnbull, in *Beam Solid Interaction and Phase Transformation,* Vol. 51 of *Materials Research Society Symposium Proceedings,* edited by H. Kurz, G. L. Olson, and J. M. Poate (MRS, Pittsburgh, 1986), p. 71.

[9]G. J. Galvin, J. W. Mayer, and P. S. Peercy, Appl. Phys. Lett. **46**, 644 (1985).

[10]F. Spaepen and D. Turnbull, in *Laser Annealing of Semiconductors,* edited by J. M. Poate and J. W. Mayer (Academic, New York, 1982).

[11]S. U. Campisano, D. C. Jacobson, J. M. Poate, A. G. Cullis, and N. G. Chew, Appl. Phys. Lett. **45**, 1216 (1984).

[12]S. U. Campisano, P. Baeri, J. P. Zhang, E. Rimini, and A. M. Malvezzi, Appl. Phys. Lett. **43**, 370 (1983).

[13]M. von Allmen and S. S. Lau, in *Laser Annealing of Semiconductors,* edited by J. M. Poate and J. M. Mayer (Academic, New York, 1982).

[14]J. H. Perepezko, D. M. Follstaedt, and P. S. Peercy, in *Beam-Solid Interaction and Transient Processes,* Vol. 74 of *Materials Research Society Symposium Proceedings,* edited by M. O. Thompson, S. T. Picraux, and J. S. Williams (MRS, Pittsburgh, 1987), p. 161.

[15]P. Baeri, G. Foti, M. G. Grimaldi, F. Priolo, and R. Reitano, in *Fundamentals of Beam-Solid Interaction and Transient Thermal Processing,* Vol. 100 of *Materials Research Society Symposium Proceedings,* edited by M. J. Aziz, L. E. Rehn, and B. Stritzker (MRS, Pittsburgh, 1988), p. 615.

[16]C. W. White, S. R. Wilson, B. R. Appleton, F. W. Young, and J. Narayan, in *Laser and Electron Beam Processing of Materials,* edited by C. W. White and P. S. Peercy (Academic, New York, 1980), p. 111.

[17]G. E. Jellison, D. H. Lowndes, D. N. Mashburn, and R. F. Wood, in *Beam-Solid Interaction and Phase Transformation,* Vol. 51 of *Materials Research Society Symposium Proceedings,* edited by H. Kurz, G. L. Olson, and J. M. Poate (MRS, Pittsburgh, 1986), p. 143.

[18]P. Baeri and S. U. Campisano, in *Laser Annealing of Semiconductors,* edited by J. M. Poate and J. W. Mayer (Academic, New York, 1982).

[19]G. E. Jellison, F. A. Modine, C. W. White, R. F. Wood, and R. T. Young, Phys. Rev. Lett. **46**, 1414 (1981).

[20]P. S. Peercy, M. O. Thompson, and J. Y. Tsao, Appl. Phys. Lett. **47**, 244 (1985).

[21]G. H. Gilmer, Mater. Sci. Eng. **65**, 15 (1984).

[22]J. Q. Broughton, G. H. Gilmer, and K. A. Jackson, Phys. Rev. Lett. **49**, 1496 (1982).

[23]I. Barin, O. Knake, and O. Kubaskewski, *Thermochemical Properties of Inorganic Substances,* Suppl. (Springer-Verlag, Berlin, 1977).

[24]S. Horiba, Z. Phys. Chem. **106**, 295 (1923).

[25]C. D. Thurmond, J. Phys. Chem. **57**, 827 (1953).

[26]V. I. Belousov, Russ. J. Phys. Chem. **53**, 1266 (1979).

[27]M. V. Rao and W. A. Tiller, J. Phys. Chem. Solids **31**, 191 (1970).

[28]A. R. Miedema, J. Less-Common. Met. (to be published).

[29]J. W. Chan, S. R. Corriel, and W. J. Boettinger, in *Laser and Electron Beam Processing of Materials,* edited by C. W. White and P. S. Peercy (Academic, New York, 1980), p. 89.